Anomalous interactions in confined charge-stabilized colloid

2004 J. Phys.: Condens. Matter 16 S4145

(http://iopscience.iop.org/0953-8984/16/38/028)

INSTITUTE OF PHYSICS PUBLISHING JOURNAL OF PHYSICS: CONDENSED MATTER

J. Phys.: Condens. Matter **16** (2004) S4145–S4157 PII: S0953-8984(04)79174-2

Anomalous interactions in confined charge-stabilized colloid

D G Grier[1] **and Y Han**[2]

[1] Department of Physics and Center for Soft Matter Physics, New York University, 4 Washington Place, New York, NY 10003, USA
[2] Department of Physics and Astronomy, University of Pennsylvania, 209 South 33rd Street, Philadelphia, PA 19104, USA

E-mail: david.grier@nyu.edu

Received 10 April 2004
Published 10 September 2004
Online at stacks.iop.org/JPhysCM/16/S4145
doi:10.1088/0953-8984/16/38/028

Abstract

Charge-stabilized colloidal spheres dispersed in weak 1:1 electrolytes are supposed to repel each other. Consequently, experimental evidence for anomalous long-ranged like-charged attractions induced by geometric confinement inspired a burst of activity. This has largely subsided because of nagging doubts regarding the experiments' reliability and interpretation. We describe a new class of thermodynamically self-consistent colloidal interaction measurements that confirm the appearance of pairwise attractions among colloidal spheres confined by one or two bounding walls. In addition to supporting previous claims for this as-yet unexplained effect, these measurements also cast new light on its mechanism.

(Some figures in this article are in colour only in the electronic version)

1. Introduction

A long-lived controversy was ignited 20 years ago by the suggestion [1, 2] that similarly charged colloidal spheres need not repel each other as predicted by Poisson–Boltzmann mean field theory [3, 4], but rather might experience a long-ranged attraction for each other under some circumstances. Interest in this problem deepened when direct measurements of colloidal interactions revealed just such attractions in micrometre-scale colloid in aqueous dispersions at extremely low ionic strength [5]. Subsequent measurements demonstrated that such anomalous like-charge attractions are only evident among spheres confined by nearby charged surfaces, and not otherwise [6–8]. This observation effectively refuted the originally proposed mechanism for like-charge colloidal attractions [8, 9], and other mean-field mechanisms were excluded soon thereafter on theoretical grounds [10–13].

When the search for more sophisticated attraction-generating mechanisms subsequently failed to reach consensus, the experimental evidence came under renewed critical scrutiny. Measurements of long-ranged attractions performed with optical tweezers near a single charged wall [14] were demonstrated to have been sensitive to a previously unsuspected kinematic coupling mechanism [15–17]. Suspicion thus was cast on all interaction measurements based on optical tweezer manipulation in confined geometries [18]. Complementary interaction measurements performed on colloidal dispersions in equilibrium are immune to kinematic artefacts [5, 19–21, 16, 22]. However, they obtain pair potentials by inverting measured pair correlation functions, a process involving various poorly controlled approximations. It is conceivable that these methods could misinterpret oscillatory many-body correlations as attractive or even oscillatory pair interactions [22]. Indeed, when particular care was taken to avoid such artefacts in measurements on a carefully prepared model system, no sign of anomalous attractions was seen [16]. These observations raise a disturbing question: could the entire case for confinement-induced like-charge attractions be based on experimental artefacts?

This article describes a new series of equilibrium colloidal interaction measurements featuring novel tests for thermodynamic self-consistency. These measurements explicitly address all of the aforementioned sources of experimental error and yield equilibrium pair potentials with quantitative error estimates. Their results confirm that confinement by one or two nearby glass walls induces long-range equilibrium attractions between nearby pairs of charged spheres. Confinement-induced attractions appear both among the highly charged polystyrene sulfate spheres that were the subject of the original round of experiments, and also between more weakly charged silica spheres. Trends observed with variations in confinement and electrolyte concentration shed new light on the attractions' origin, suggesting a role for non-monotonic correlations in the distribution of simple ions near charged surfaces.

2. The structure of colloidal monolayers

Our colloidal interaction measurements follow the general approach pioneered by Kepler and Fraden [5] and Vondermassen *et al* [19], in which digital video microscopy is used to measure the distribution of spheres in a dispersion at equilibrium. Figure 1 shows our implementation schematically. An aqueous charge-stabilized dispersion fills a hermetically sealed slit pore between a glass microscope slide and a coverslip. The confined dispersion is allowed to equilibrate with reservoirs of mixed-bed ion exchange resin to a base concentration of roughly 1 μM. Controlling the pressure of a buffer gas in these reservoirs also permits the spacing H between the walls to be adjusted and maintained constant over the course of an hour-long measurement [8]. Residual contaminant ions are believed to consist of sodium ion leached from the glass, and carbonate infiltrating from the atmosphere, both of which are monovalent. The glass surfaces develop large negative charge densities [17] that repel negatively charged colloidal spheres and prevent them from sticking under the influence of van der Waals attraction. Depending on the resulting balance of forces on the spheres, the dispersion can be confined to a monolayer at height h above the lower surface.

Spheres larger than a few hundred nanometres in diameter are readily imaged by conventional bright-field microscopy. A detail from a typical video micrograph of $\sigma = 1.58\ \mu$m diameter silica spheres appears in figure 1. The spheres' centres can be tracked with standard techniques of digital video microscopy [7], with accuracies of $\Delta x = \Delta y = 30$ nm being achieved for these particles [23, 24]. The plot in figure 1 shows the trajectory of a single sphere over one minute from the region indicated by the box overlaid on the micrograph.

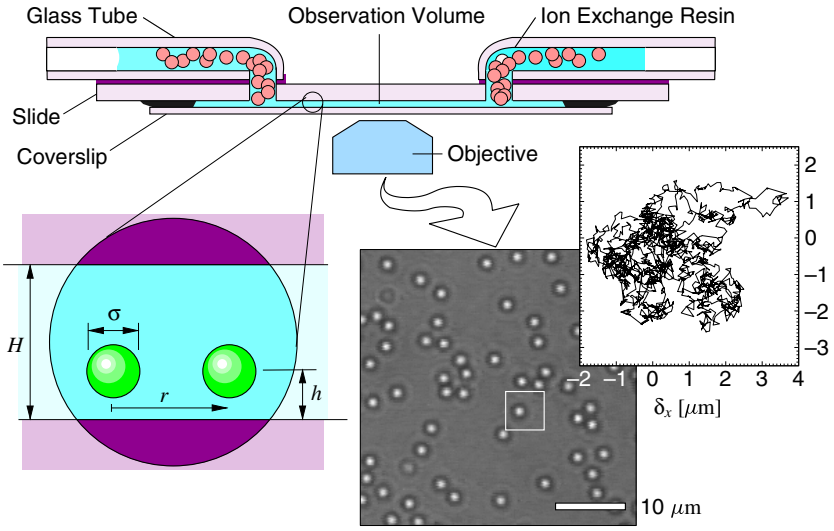

Figure 1. Measuring the structure of colloidal monolayers.

The in-plane positions, $\mathbf{r}_j(t)$, of spheres labelled by j in snapshots obtained over time t can be compiled into the time-dependent particle density

$$\rho(\mathbf{r}, t) = \sum_{j=1}^{N(t)} \delta(\mathbf{r} - \mathbf{r}_j(t)). \tag{1}$$

The rest of our results are extracted from $\rho(\mathbf{r}, t)$.

For example, individual trajectories can be analysed with the Einstein–Smoluchowsky relation

$$P(\delta_k|t) = \exp\left(-\frac{(\delta_k - v_k t)^2}{2D_k t}\right), \tag{2}$$

which describes the probability of finding particles displaced by distance $\delta_k = \langle \mathbf{r}_j(t) - \mathbf{r}_j(0)\rangle_k$ along the kth coordinate after time t. Fitting to equation (2) yields the particles' diffusion coefficients D_k and mean drift velocities v_k. For an equilibrated isotropic system, we expect identical diffusion coefficients in orthogonal directions and no overall drift. These conditions are met for all of the data sets presented below, with maximum drift speeds below 0.3 μm s^{-1} and typical speeds far smaller.

Provided care is taken to account for the finite field of view and the varying number $N(t)$ of particles within it [25, 16, 23], $\rho(\mathbf{r}, t)$ can be summarized with the radial distribution function

$$g(r) = \frac{1}{n^2}\left\langle \frac{\rho(\mathbf{r} - \mathbf{r}', t)\rho(\mathbf{r}', t)}{A(\mathbf{r})} \right\rangle, \tag{3}$$

where the angle brackets indicate an average over the field of view, over angles, and over time, and where $n = N/A$ is the areal density of $N = \langle N(t)\rangle$ particles in area A, and $A(\mathbf{r})$ is the area within the field of view over which pairs separated by $\mathbf{r}$ might be found.

3. Liquid structure inversion

The Boltzmann formula,

$$g(r) = \exp(-\beta w(r)), \tag{4}$$

relates the radial distribution function for an isotropic system in equilibrium to the potential of mean force $w(r)$ associated with its structure. Here, $\beta^{-1} = k_{\mathrm{B}}T$ is the thermal energy scale at absolute temperature T. The potential of mean force can be identified with the system's underlying pair potential only in the limit of infinite dilution,

$$u(r) = \lim_{n\to 0} w(r). \tag{5}$$

At higher densities, simple crowding can induce layering, and thus oscillatory correlations, even in a system whose pair interactions are monotonically repulsive. Interpreting the effective inter-colloid interaction is still more problematic. The spheres' dynamics reflect not only their direct Coulomb repulsions, but also the influence of a sea of atomic scale simple ions, whose distribution also depends on the spheres' comparatively enormous charges and excluded volumes. The effective interaction between two spheres reflects a thermodynamic average over the simple ions' degrees of freedom. This almost certainly will depend on the distribution of other spheres at higher sphere concentrations. Under such circumstances, the effective pair potential would not be well defined. At lower concentrations, however, the dispersion's free energy can be described as a superposition of pairwise interactions.

For all of these reasons, non-monotonic dependence of $\beta w(r) = -\ln g(r)$ on separation r need not signal the onset of attractive interactions. Particularly in systems with long-ranged repulsive interactions, care must be taken to correct for many-body correlations. Unfortunately, no exact relationship is known between $u(r)$ and $w(r)$ at finite concentrations, even if the functional form of $u(r)$ is available. Instead, two strategies for inverting $g(r)$ have emerged, one involving molecular dynamics or Monte Carlo simulations to refine trial pair potentials [5, 26], and the other exploiting results from liquid structure theory to correct for many-body correlations [20, 16]. The results from either approach may be identified with the underlying pair potential thanks to Henderson's uniqueness theorem [27].

We will avail ourselves of the Ornstein–Zernicke liquid structure formalism to invert $g(r)$ [28], building upon the pioneering work of Carbajal-Tinoco *et al* [20]. When applied to the spheres in a colloidal dispersion, the Ornstein–Zernicke equation describes how effective interactions among neighbouring spheres give rise to structural correlations. In principle, it describes a hierarchy of N-body correlations emerging from pairwise interactions. Truncating the hierarchy yields analytically tractable approximations, whose predictions are increasingly accurate at lower densities. Two of these approximations, the hypernetted chain (HNC) and Percus–Yevick (PY) equations, have been found to accurately describe the structure emerging from computer simulations of systems with long-range (HNC) and short-range (PY) interactions. For two-dimensional systems, these are most conveniently expressed as

$$\beta u(r) = \beta w(r) + \begin{cases} nI(r) & \text{(HNC)} \\ \ln[1 + nI(r)] & \text{(PY)}, \end{cases} \tag{6}$$

where the convolution integral

$$I(r) = \int \big[g(r') - 1 - nI(r)\big]\big[g(|\mathbf{r}' - \mathbf{r}|) - 1\big]\,\mathrm{d}^2r' \tag{7}$$

can be solved iteratively, starting with $I(r) = 0$ [29]. Evaluating $I(r)$ directly rather than with numerical Fourier transforms minimizes the sensitivity of $u(r)$ to noise in $g(r)$. This implementation has been shown to be both accurate and effective in previous related studies [16, 23, 24].

4. Interactions and the DLVO theory

Figure 2 shows typical results for pair potentials obtained from measured radial distribution functions with both the HNC and PY approximations. The data plotted as circles in figure 2(a)

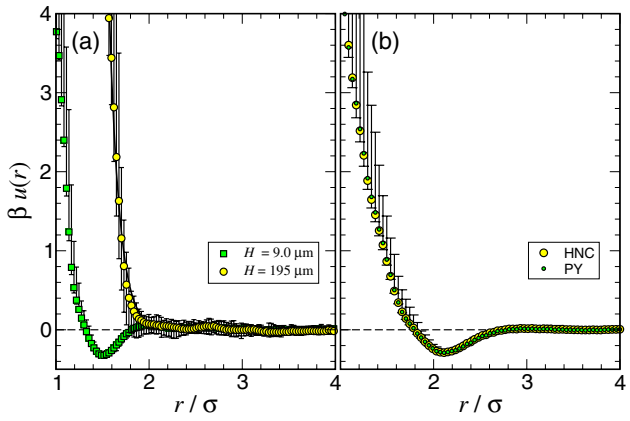

Figure 2. Measured interactions in confined monolayers of (a) silica spheres $\sigma = 1.58$ μm in diameter and (b) polystyrene spheres $\sigma = 0.652$ μm in diameter. The silica spheres are sedimented into a monolayer at height $h = 0.9$ μm above the lower wall. The two data sets in (a) were obtained at areal density $n\sigma^2 = 0.0654$ for $H = 9$ μm and $n\sigma^2 = 0.0797$ for $H = 195$ μm. The polystyrene spheres, by contrast, are confined to the midplane between parallel glass walls separated by $H = 1.3$ μm, with $n\sigma^2 = 0.056$.

were obtained for silica spheres $\sigma = 1.58$ μm in diameter in slit pores of height $H = 195$ and 9 μm. Silica's density is twice that of water, and these spheres sediment into a monolayer with their centres at $h = 0.9$ μm above the lower glass wall, with out-of-plane excursions estimated [16] to be no greater than $\delta h = 0.1$ μm. This system was originally proposed as a model for studying attractions mediated by a single wall in equilibrium [16]. Indeed, the data obtained for a confined monolayer at $H = 9$ μm exhibit a strong and long-ranged attraction [23]. The pair potential measured at $H = 195$ μm, however, is monotonically repulsive [16, 23]. This observation raises substantial questions regarding the nature of the more distant wall's influence.

The purely repulsive potential in figure 2(a) is described very well by the screened-Coulomb form predicted by the classic Derjaguin–Landau–Verwey–Overbeek linearized mean-field model for colloidal electrostatic interactions [3, 4]:

$$\beta u(r) = Z^2 \lambda_B \left(\frac{\exp(\kappa a)}{1 + \kappa a} \right)^2 \frac{\exp(-\kappa r)}{r}. \tag{8}$$

Here, Z is the effective valence of a sphere of radius $a = \sigma/2$, $\lambda_B = \beta e_0^2/(4\pi\epsilon)$ is the Bjerrum length for a medium of dielectric constant ϵ at temperature T, where e_0 is the elementary charge, and κ^{-1} is the Debye–Hückel screening length given by $\kappa^2 = 4\pi\lambda_B n_0$ in an electrolyte with a concentration n_0 of monovalent ions. Fitting to the $H = 200$ μm data in figure 2(a) yields a charge number $Z = 6500 \pm 1000$, in good agreement with the predictions of charge renormalization theory [17], and screening length $\kappa^{-1} = 180 \pm 10$ nm consistent with the system's estimated micromolar ionic strength. Comparable results are obtained for monolayers at areal densities ranging from $n\sigma^2 = 0.04$ to 0.10, suggesting that the result is independent of density, and that the liquid structure inversion correctly accounts for many-body correlations in this concentration range. All other results reported here were obtained under comparable conditions.

The observation of DLVO-like repulsions in a weakly confined silica monolayer is consistent with previous reports on this system [16]. It also demonstrates that our methods do not necessarily yield non-monotonic potentials in this range of experimental conditions. When

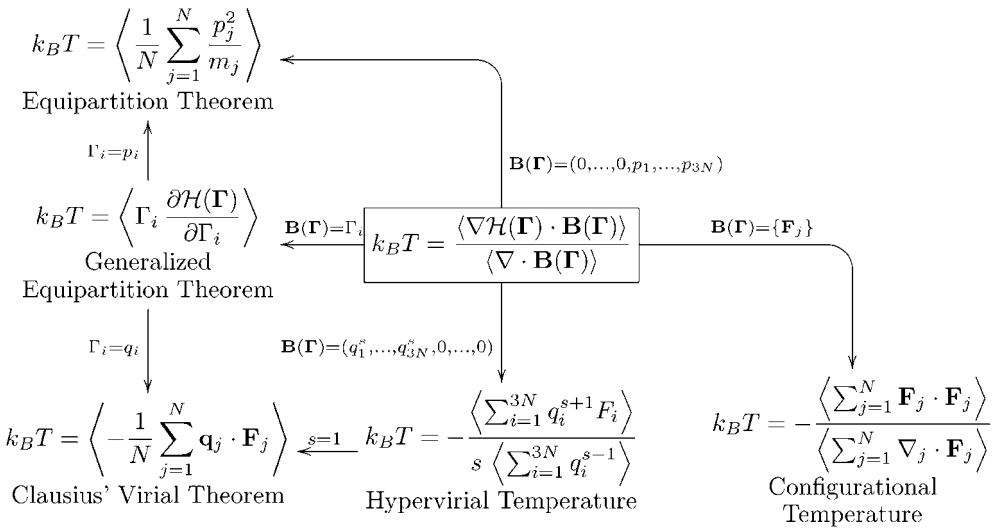

Figure 3. Various consequences of the generalized temperature definition for selected choices of the arbitrary vector field $\mathbf{B}(\mathbf{\Gamma})$.

viewed in this light, the appearance of an attractive minimum in the pair potential for the more tightly confined but otherwise identical monolayer at $H = 9\ \mu$m seems more credible than it otherwise might [23, 24]. The observation of attractions in silica colloid breaks the monopoly on anomalous attractions held by the substantially more highly charged polystyrene sulfate spheres used in previous studies [5, 6, 8, 20].

Such indirect verification does not make the result any less surprising, however. The potential's minimum is roughly $0.3\ k_{\mathrm{B}}T$ deep at a centre-to-centre separation of $r = 2.4\ \mu$m. The interaction's attractive component thus is substantially longer ranged than the core electrostatic repulsion, and measurably influences colloidal dynamics at distances extending to tens of screening lengths. This greatly exceeds the range of like-charge macromolecular attractions ascribed to polyvalent counterions, counterion correlations, or fluctuations in the counterion distribution. Still more puzzling is that a wall separated from the monolayer by nearly 8 μm can qualitatively transform the spheres' apparent pair potential.

Comparably strong and long-ranged attractions are evident in the data plotted in figure 2(b), which were obtained for polystyrene spheres $\sigma = 0.652\ \mu$m in diameter confined to the midplane between glass walls separated by $H = 1.3\ \mu$m. These data are consistent with all previous observations of like-charge attractions in confined polystyrene [5, 20, 8], including those involving optical tweezers [8].

As an additional reliability check, results for the polystyrene data are plotted using both the HNC and PY approximations. Their quantitative agreement suggests that the monolayer's areal density is low enough for the liquid structure formalism to account accurately for many-body correlations in $g(r)$. Indeed, there is little difference between $w(r)$ and $u(r)$ for this data set. We calculate the difference $\Delta u_{\mathrm{L}}(r)$ between the HNC and PY approximations for each data set and add it in quadrature to other sources of uncertainty to estimate errors in the reported $u(r)$.

By far the largest source of error results from experimental uncertainties in $g(r)$. These, in turn, result from errors in measuring the particle position and from counting statistics. Assessing the latter turns out to be somewhat subtle and establishes the lowest practical areal density n at which a reliable measurement can be made.

The subtlety hinges on the following question: How many snapshots are required to ascertain whether or not the particles interact at all? In other words, how many pairs would we expect to see at the centre-to-centre separation r in a non-interacting system? Given a spatial resolution $\mathrm{d}r$ for binning particle separations into the radial distribution function, this number is $2\pi n^2 A r\,\mathrm{d}r$. Typically, the number $N = nA = \mathcal{O}(100)$ of particles in the field of view A is so small that the expected number of pairs would be unacceptably small. Combining data from M statistically independent snapshots reduces the associated error in $g(r)$ to $\Delta^{(s)}g(r) = g(r)/(2\pi n^2 AMr\,\mathrm{d}r)$.

Errors due to uncertainties in particle location can be calculated as $\Delta^{(m)}g(r) = 2\,\partial_r g(r)\,\Delta x$, where Δx is the error in locating a single particle's centroid in each dimension. The radial derivative of $g(r)$ can be computed numerically from the experimental data, which is binned to resolution $\mathrm{d}r$. Typically, $\Delta x \ll \mathrm{d}r$, so that $\Delta^{(m)}g(r) \ll \Delta^{(s)}g(r)$.

Even though the particles' out-of-plane excursions are small, they also contribute to errors in $g(r)$ through projection errors, especially near contact. Out-of-plane fluctuations δh make the particles appear to be closer than they actually are. The error in apparent particle separation falls off with separation as $\Delta r = (\delta h)^2/r$. In practice, we combine this contribution in quadrature with the estimated error due to inaccuracies in particle tracking, $2\Delta x$, in computing $\Delta^{(m)}g(r)$.

Combining $\Delta^{(m)}g(r)$ and $\Delta^{(s)}g(r)$ in quadrature establishes the range of possible values of $g(r)$ for a given sample, restricted only by the requirement that $g(r) \geqslant 0$. We compute trial pair potentials in both the HNC and PY approximations using both the upper and lower bounds on $g(r)$ as inputs. The resulting lower and upper estimates on $u(r)$ then are added in quadrature with the systematic error due to differences in HNC and PY results to obtain estimates for the upper and lower error bars on $u(r)$. Typical results appear in figure 2, and establish that the minima reported in these data are indeed clearly resolved by our methods, even if the error bounds near contact are substantial.

5. Thermodynamic self-consistency: configurational temperature

Despite the care taken to estimate and eliminate sources of error in these measurements, using equations (6) and (7) to interpret experimental data might be criticized for its uncontrolled approximations: equations (6) and (7) can converge numerically to an answer even when applied well beyond their domain of validity. Assessing the bounds of this domain can be problematic if the form of the pair potential is not known *a priori*. Applying liquid structure theory to experimental data also requires the assumption of pairwise additivity. Nonadditivity, however, would have no obvious signature in the results. Other unintended processes such as nonequilibrium hydrodynamic coupling also can yield reasonable-looking results that could be mistaken for an equilibrium pair interaction [30]. Consequently, the appearance of qualitatively new features in any particular measurement of $u(r)$ could signal a failure in the method. For this reason, most published accounts have relied upon comparisons among several related systems to bolster their conclusions regarding trends in confinement-mediated interactions. These comparisons are themselves subject to question because the ultraclean chemical environments required for these studies are difficult to alter in a predictable manner.

To address all such concerns, we have introduced [24] methods to assess whether or not a trial pair potential describes a system's interactions in a thermodynamically self-consistent manner. Our approach is based on the recently introduced notion of a *configurational temperature*, which has found widespread applications in simulations [31, 32], but has not previously been applied to experimental data [24].

The temperature of an equilibrium ensemble of particles is defined conventionally in terms of the particles' mean kinetic energy, without regard for their instantaneous positions. In 1997, Rugh pointed out that the temperature can also be expressed as ensemble averages over geometrical and dynamical quantities [33]. This notion is expressed more generally [34, 35] as

$$k_{\mathrm{B}}T = \frac{\langle \nabla \mathcal{H}(\mathbf{\Gamma}) \cdot \mathbf{B}(\mathbf{\Gamma}) \rangle}{\langle \nabla \cdot \mathbf{B}(\mathbf{\Gamma}) \rangle}, \tag{9}$$

where angle brackets indicate an ensemble average, $\mathbf{\Gamma} = \{q_1, \ldots, q_{3N}, p_1, \ldots, p_{3N}\}$ is the instantaneous set of $3N$ generalized coordinates q_j and their conjugate momenta p_j for an N-particle system, $\mathcal{H}(\mathbf{\Gamma}) = \sum_{j=1}^{3N} p_j^2/(2m) + V(\{q_j\})$ is the Hamiltonian associated with the conservative N-particle potential $V(\{q_j\})$, and $\mathbf{B}(\mathbf{\Gamma})$ is an *arbitrary* vector field selected so that both the numerator and denominator of equation (9) are finite and the numerator grows more slowly than e^N in the thermodynamic limit. Figure 3 shows inter relationships among results obtained with several choices for $\mathbf{B}(\mathbf{\Gamma})$. For instance, choosing $\mathbf{B}(\mathbf{\Gamma}) = \{0, \ldots, 0, p_1, \ldots p_{3N}\}$ yields the familiar equipartition theorem. Choosing instead $\mathbf{B}(\mathbf{\Gamma}) = -\nabla V(\{q_i\})$ yields a formally equivalent result,

$$k_{\mathrm{B}}T_{\mathrm{config}} = \frac{\langle |\nabla V|^2 \rangle}{\langle \nabla^2 V \rangle}, \tag{10}$$

which depends only on the particles' instantaneous configuration, and not on their momenta.

Directly applying equation (10) requires the full N-particle free energy, which is rarely available. Simplified forms emerge for systems satisfying certain conditions. For example, if $V(\{q_i\})$ is the linear superposition of pair potentials, $u(r)$, then equation (10) reduces to [31]

$$k_{\mathrm{B}}T_{\mathrm{conF}} = -\frac{\left\langle \sum_{i=1}^{N} F_i^2 \right\rangle}{\left\langle \sum_{i=1}^{N} \nabla_i \cdot \mathbf{F}_i \right\rangle}, \tag{11}$$

where $\mathbf{F}_i = -\sum_{j \neq i} \nabla_i u(r_{ij})$ is the total force on particle i due to its interactions with other particles, ∇_i is the gradient with respect to the ith particle's position, $\mathbf{r}_i$, and $r_{ij} = |\mathbf{r}_i - \mathbf{r}_j|$ is the centre-to-centre separation between particles i and j. The temperature is reflected in the instantaneous distribution of forces because objects explore more of their potential energy landscape as the temperature increases.

Equation (11) may be generalized into a hierarchy of *hyperconfigurational* temperatures by choosing $\mathbf{B}(\mathbf{\Gamma}) = \{F_i^s\}$:

$$k_{\mathrm{B}}T_{\mathrm{h}}^{(s)} = -\frac{\left\langle \sum_{i=1}^{N} F_i^{s+1} \right\rangle}{\left\langle s \sum_{i=1}^{N} F_i^{s-1} \nabla_i \cdot \mathbf{F}_i \right\rangle}, \tag{12}$$

for $s > 0$. These higher moments are more sensitive to the input potential's detailed structure than $T_{\mathrm{conF}} = T_{\mathrm{h}}^{(1)}$. They also can be applied to three-dimensional systems with long-ranged $1/r$ potentials, for which T_{conF} is ill-defined. Equations (9)–(12) apply only in the thermodynamic limit, with errors of $\mathcal{O}(1/N)$.

For systems with short-ranged potentials, dropping additional terms of $\mathcal{O}(1/N)$ from equation (9) yields [34]

$$k_{\mathrm{B}}T_{\mathrm{con1}} = -\left\langle \frac{\sum_{i=1}^{N} F_i^2}{\sum_{i=1}^{N} \nabla_i \cdot \mathbf{F}_i} \right\rangle, \tag{13}$$

and

$$k_{\mathrm{B}}T_{\mathrm{con2}} = -\left\langle \frac{\sum_{i=1}^{N} \nabla_i \cdot \mathbf{F}_i}{\sum_{i=1}^{N} F_i^2} \right\rangle^{-1}, \tag{14}$$

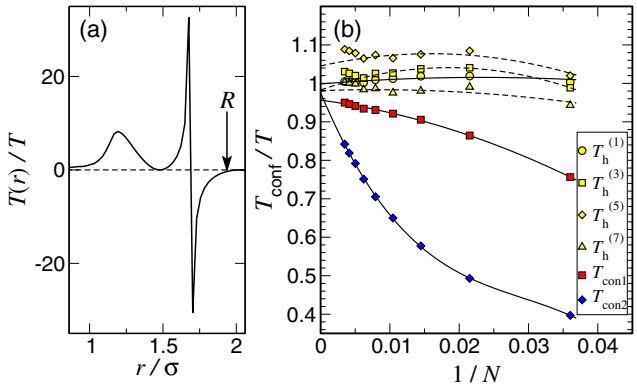

Figure 4. (a) Estimating the range over which interactions affect the configurational temperature for the silica data at $H = 9\ \mu$m. (b) Finite-size scaling of several variants of the configurational temperature for the silica data at $H = 9\ \mu$m. Solid curves are fits to third-order polynomials in $1/N$ showing extrapolations to the thermodynamic limit.

the second of which was proposed in [24]. These definitions' different dependences on sample size N are useful for comparison with $T_{\mathrm{h}}^{(s)}$.

We apply the configurational temperature formalism to our colloidal monolayers by using the measured particle locations $\rho(\mathbf{r}, t)$ and extracted pair potential $u(r)$ as inputs to the various definitions. Provided that the conditions for the configurational temperatures' derivation are met, then all variants will yield results consistent with each other and with the (known) temperature T of the heat bath. In particular, consistent results emerge only if the system is in local thermodynamic equilibrium, if its interactions are indeed pairwise additive, and if the measured pair potential $u(r)$ accurately reflects those interactions.

In practice, each snapshot of a monolayer's configuration constitutes a measurement of its configurational temperature. Particles near the edge of the field of view, however, may have strongly interacting neighbours just out of the field of view whose contributions to their net force would be overlooked. Including these apparently unbalanced forces would grossly distort estimates of the configurational temperature. To avoid this, we calculate force distributions only for particles whose relevant neighbours all lie within the field of view. Such particles lie no closer than the interaction's range R to the edge of the field of view. We estimate R from $u(r)$ and $g(r)$ by computing

$$\frac{T(r)}{T} = 2\pi\beta\frac{r}{\sigma}g(r)\frac{|\nabla u(r)|^2}{\nabla^2 u(r)}, \tag{15}$$

an example of which is plotted in figure 4(a). This function may be interpreted as the contribution to the configurational temperature due to particles separated by distance r. Quite clearly, pairs with $r > R \approx \sigma$ contribute little if at all to the configurational temperature.

Truncating the field of view to avoid edge effects further reduces the number N of particles in the field of view. This is problematic because all of the temperature definitions involve approximations of $\mathcal{O}(1/N)$. Adopting a standard technique from simulation studies, we deliberately subsample the available data, recalculate the configurational temperature on the restricted data set, and extrapolate to the large N limit by fitting the result to a polynomial in $1/N$. Typical results appear in figure 4(b). Even though the different definitions have substantially different dependences on sample size, they all extrapolate to the thermodynamic temperature in the thermodynamic limit.

This result turns out to be reassuringly sensitive to details of the pair potential. The small residual scatter in the experimental $u(r)$ is greatly magnified in calculating the configurational temperature, particularly for the higher-order hyperconfigurational temperatures. Consequently, the data in figure 2 were fitted to a fifth-order polynomial whose coefficients were used in calculating the results shown in figure 4. Varying the pair potential by as little as 1% in the region of the core repulsion increases the apparent configurational temperature by more than 10%. Simply truncating the attractive minimum in $u(r)$ to mimic a purely repulsive potential leads to a 50% increase, or an error of 150 °C.

The successful collapse of the configurational and hyperconfigurational temperatures to the thermodynamic temperature constitutes a set of stringent internal self-consistency tests for the accuracy of the measured pair potential and its correct interpretation. When combined with the considerations from the previous sections, we can improve the estimated resolution of our pair potential to roughly $1/20\ k_{\mathrm{B}}T$. The observed confinement-induced attractions therefore should be considered a real, pairwise additive contribution to the monolayers' free energy, at least in this range of ionic strength and areal density.

6. The role of confinement

We next investigate the role of geometric confinement in inducing like-charge attractions in sedimented silica monolayers. Figure 5 shows data from five different monolayers of silica spheres ($\sigma = 1.58\ \mu$m) in slit pores ranging in depth from $H = 195\ \mu$m down to $3.2\ \mu$m. Figure 5(b) shows the associated configurational temperatures. For all inter-wall separations, the monolayer is sedimented at roughly $h = 900$ nm, with the only obvious difference being the inter-wall spacing. Well-resolved attractive minima are evident for plate separations as large as $H = 30\ \mu$m.

This observation contrasts with measurements on more highly charged polystyrene sulfate spheres, for which anomalous attractions appear only when the spheres are rigidly confined to the midplane, at separations no larger than $H = 4\sigma$ [8]. This difference may be due to the silica spheres' proximity to the lower wall. Why then would attractions not be evident at $H = 200\ \mu$m [16, 23, 24]? More to the point, why would a second wall at $H = 20\sigma$ make a difference? Trends in figure 5(a) suggest an explanation.

One prominent feature of these data sets is that the apparent range of the core repulsion moves monotonically to smaller r as the inter-wall separation decreases. This differs from the results of optical tweezer measurements on polystyrene spheres, in which the depth of the attractive minimum varies with H, but not the range of the repulsion [8]. It is tempting to ascribe the trend in our silica data to a decrease in the effective Debye–Hückel screening length as the ratio of surface area to volume increases and diffusive contact with the ion exchange reservoirs diminishes. If this were the case, however, we would expect the slope of $u(r)$ near contact to decrease monotonically also. Instead, there is no discernible trend.

Referring to the DLVO result in equation (8) for guidance, it would appear that the spheres' effective charge Z is the only other parameter that might be free to vary. Such variation is consistent, at least qualitatively, with the predictions of charge renormalization theory [17] for silica spheres near charged silica surfaces. It would also explain the different behaviour of polystyrene spheres whose more acidic surface groups are not so susceptible to charge regulation by nearby surfaces [17]. However, it leaves open the question of why an attraction appears at all.

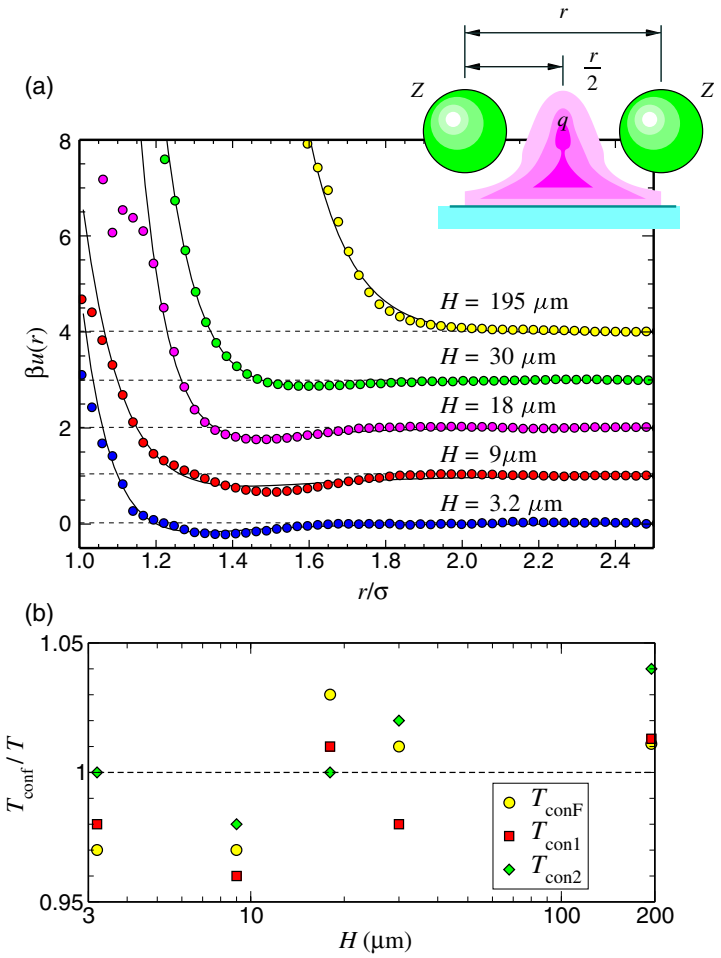

Figure 5. (a) Measured pair potentials for monolayers of silica spheres 1.58 μm in diameter sedimented to a height $h = 900 \pm 100$ nm above a glass surface for a variety of inter-wall separations, H. The solid curves are fits to equation (16) with parameters tabulated in table 1. The inset schematically represents the space charge model for confinement-induced attractions. (b) Configurational temperatures for each of the interaction measurements.

7. Speculation: space-charge mediated attractions

A variety of mechanisms beyond Poisson–Boltzmann mean field theory have been proposed for confinement-induced attractions among like-charged colloid. These include attempts to compute London-like attractions due to fluctuations in the distribution of simple ions around the large spheres [36] and density functional analysis of high-order correlations in the distribution of large and small ions [37, 18]. The few that appear to reproduce experimental observations [38, 37] have proved controversial [39, 40], and none of the more widely accepted calculations predicts an attraction of the range and strength observed experimentally, particularly if the simple ions are monovalent. Nor have computer simulations yet been able to address the regime of large charge asymmetry that appears to be necessary for this effect. Other approaches, however, may shed light on these anomalous interactions.

Table 1. Interaction parameters obtained from fits to the space charge model.

H (μm)	Z	κ^{-1} (μm)	q
195	7000 ± 400	200 ± 20	3 ± 3
30	2500 ± 150	160 ± 20	10 ± 2
18	2400 ± 150	140 ± 20	13 ± 3
9	800 ± 100	150 ± 25	13 ± 4
3.2	800 ± 100	150 ± 20	11 ± 2

The Kirkwood–Poirer formulation of electrolyte structure [41], for example, suggests that the correlations between macroions and simple ions can become non-monotonic in the strongly coupled regime. Hastings subsequently pointed out that these correlations in the simple ion distribution would lead to local violations of electroneutrality in regions between macroions [42], and that the resulting effective interaction between macroions would include an attractive component. This result parallels the more recent thermodynamically consistent liquid structure calculation by Carbajal-Tinoco and Gonzalez-Mozuelos [43].

If we hypothesize that the distribution of counterions extending away from a charged surface also develops regions of space charge when modulated by nearby spheres, then the effective inter-sphere interaction should include a term accounting for sphere–space charge–sphere bridging. In the absence of a theory for the actual simple ion distribution, we model the space charge's influence as the screened coulomb interaction between the spheres' effective charges and a point charge of valence q centred between them:

$$\beta u(r) = Z^2 \lambda_B \left(\frac{\exp(\kappa a)}{1+\kappa a} \right)^2 \frac{\exp(-\kappa r)}{r} - 4Zq\lambda_B \frac{\exp(\kappa a)}{1+\kappa a} \frac{\exp\left(-\frac{1}{2}\kappa r\right)}{r}. \tag{16}$$

Fitting the data in figure 5(a) to this form yields remarkably good agreement, with fitting parameters tabulated in table 1. The screening lengths in all cases are consistent with the expected micromolar ionic strengths of our apparatus. The spheres' effective charge number appears to decrease systematically with wall separation in a manner at least qualitatively consistent with charge regulation theory [17]. Most tellingly, the effective space charge number is consistent with $q = 10$ at all separations. If this model is to be taken seriously, this result suggests that the sedimented silica spheres are indeed influenced by the nearby wall's counterion distribution, and that the resulting attraction is evident only when the core electrostatic repulsion is not too strong. Reducing the spheres' effective charge exposes the nascent attraction in this scenario. For the more highly charged polystyrene spheres, reducing the wall separation has little effect on the spheres' effective charge or the screening length, but increases the concentration of counterions between the spheres.

This simple space-charge model appears to account for the available observations of like-charge attractions between confined charge-stabilized spheres. Its interpretation points toward a correlation-based explanation for the effect, albeit of an extraordinary range. The measurements described in the present work should help to eliminate any remaining concerns regarding the validity and accuracy of the larger body of measurements in the literature, and their interpretation. The thermodynamically self-consistent measurement protocol we introduce should also find applications in the broader context of experimental soft matter research.

Acknowledgment

This work was supported by the donors of the Petroleum Research Fund of the American Chemical Society.

References

[1] Sogami I 1983 *Phys. Lett.* A **96** 199
[2] Sogami I and Ise N 1984 *J. Chem. Phys.* **81** 6320
[3] Derjaguin B V and Landau L 1941 *Acta Physicochim. (URSS)* **14** 633
[4] Verwey E J and Overbeek J T G 1948 *Theory of the Stability of Lyophobic Colloids* (Amsterdam: Elsevier)
[5] Kepler G M and Fraden S 1994 *Phys. Rev. Lett.* **73** 356
[6] Crocker J C and Grier D G 1994 *Phys. Rev. Lett.* **73** 352
[7] Crocker J C and Grier D G 1996 *J. Colloid Interface Sci.* **179** 298
[8] Crocker J C and Grier D G 1996 *Phys. Rev. Lett.* **77** 1897
[9] Grier D G and Crocker J C 2000 *Phys. Rev.* E **61** 980
[10] Neu J C 1999 *Phys. Rev. Lett.* **82** 1072
[11] Sader J E and Chan D Y C 1999 *J. Colloid Interface Sci.* **213** 268
[12] Sader J E and Chan D Y C 2000 *Langmuir* **16** 324
[13] Trizac E 2000 *Phys. Rev.* E **62** 1
[14] Larsen A E and Grier D G 1997 *Nature* **385** 230
[15] Squires T and Brenner M P 2000 *Phys. Rev. Lett.* **85** 4976
[16] Behrens S H and Grier D G 2001 *Phys. Rev.* E **64** 050401
[17] Behrens S H and Grier D G 2001 *J. Chem. Phys.* **115** 6716
[18] Attard P 2001 *Curr. Opin. Colloid Interface Sci.* **6** 366
[19] Vondermassen K, Bongers J, Mueller A and Versmold H 1994 *Langmuir* **10** 1351
[20] Carbajal-Tinoco M D, Castro-Román F and Arauz-Lara J L 1996 *Phys. Rev.* E **53** 3745
[21] Bongers J, Manteufel H, Vondermaßen K and Versmold H 1998 *Colloids Surf.* A **142** 381
[22] Brunner M, Bechinger C, Strepp W, Lobaskin V and von Grunberg H H 2002 *Europhys. Lett.* **58** 926
[23] Han Y and Grier D G 2003 *Phys. Rev. Lett.* **91** 038302
[24] Han Y and Grier D G 2004 *Phys. Rev. Lett.* **92** 148301
[25] Bongers J, Manteufel H, Versmold H and Vondermaßen K 1998 *J. Chem. Phys.* **108** 9937
[26] Rajagopalan R and Rao K S 1997 *Phys. Rev.* E **55** 4423
[27] Duh D M and Henderson D 1996 *J. Chem. Phys.* **104** 6742
[28] McQuarrie D A 2000 *Statistical Mechanics* (Mill Valley, CA: University Science Books)
[29] Chan E M 1977 *J. Phys. C: Solid State Phys.* **10** 3477
[30] Squires T M 2001 *J. Fluid Mech.* **443** 403
[31] Butler B D, Ayton G, Jepps O G and Evans D J 1998 *J. Chem. Phys.* **109** 6519
[32] Delhommelle J and Evans D J 2002 *J. Chem. Phys.* **117** 6016
[33] Rugh H H 1997 *Phys. Rev. Lett.* **78** 772
[34] Jepps O G, Ayton G and Evans D J 2000 *Phys. Rev.* E **62** 4757
[35] Rickayzen G and Powles J G 2001 *J. Chem. Phys.* **114** 4333
[36] Gopinathan A, Zhou T, Coppersmith S N, Kadanoff L P and Grier D G 2002 *Europhys. Lett.* **57** 451
[37] Goulding D and Hansen J P 1999 *Europhys. Lett.* **46** 407
[38] Goulding D and Hansen J P 1999 *Mol. Phys.* **95** 649
[39] Trizac E and Raimbault J L 1999 *Phys. Rev.* E **60** 6530
[40] Mateescu E M 2001 *Phys. Rev.* E **64** 013401
[41] Kirkwood J G and Poirier J C 1954 *J. Chem. Phys.* **58** 591
[42] Hastings R 1978 *J. Chem. Phys.* **68** 675
[43] Carbajal-Tinoco M D and Gonzalez-Mozuelos P 2002 *J. Chem. Phys.* **117** 2344